Effect of irradiation on nanoprecipitation in EM10 alloy - Comparison with Eurofer97

O. Tissot, G. Sakr, Cristelle Pareige, J. Henry

Effect of irradiation on nanoprecipitation in EM10 alloy - Comparison with Eurofer97

O. Tissot [a, *], G. Sakr [a], C. Pareige [b], J. Henry [a]

[a] DEN-Service de Recherches Métallurgiques Appliquées, CEA, Université Paris-Saclay, F-91191, Gif-sur-Yvette, France
[b] Normandie Univ, UNIROUEN, INSA Rouen, CNRS, Groupe de Physique des Matériaux, 76000, Rouen, France

A B S T R A C T

Atom Probe Tomography investigations of EM10 and EUROFER alloys after both 1 MeV electrons and 2 MeV Fe^{2+} ions irradiations at 300 °C and up to doses of 0.6 dpa were performed. SiNiPMn(-Cu) enriched clusters were observed only in EM10 alloy. Phosphorus was found to be necessary for cluster formation. Segregation of Si, Ni, P, Mn elements were measured at a Grain Boundary and a dislocation. Cr clusters near a dislocation were noticed.

Keyworas:
Ferritic/martensitic
Electrons irradiation
Ions irradiation
Precipitation
Segregation
Atom Probe Tomography (APT)

1. Introduction

The 9Cr–1Mo EM10 tempered martensitic alloy is a candidate for future application in GEN IV reactors. In particular, its characteristics make it a reference material for the hexagonal duct of future Generation IV Sodium-cooled Fast Reactor [1]. EM10 presents very good resistance to swelling up to 100 dpa at least and exhibits dimensional stability up to 550 °C under neutron irradiation [2,3].

For fusion applications, Ferritic Martensitic (FM) steels with reduced activation properties, for instance the 9Cr–1WVTa EUROFER steel, are preferred to conventional FM steels like EM10. For instance, EUROFER was selected as reference material in Europe for the fusion reactor DEMO [4]. It is well established that FM steels like EM10 and EUROFER exhibit pronounced hardening when irradiated at low temperatures, typically below 400 °C, due in particular to the formation of a high density of radiation-induced dislocation loops [5]. However, the increase in yield stress was found to be significantly higher in EM10 compared to EUROFER after neutron irradiation at 325 °C to 78 dpa [6]. Owing to their relatively low Cr content, it is believed that α-α' unmixing is not a major contribution to irradiation induced hardening in EUROFER and EM10. However, while EUROFER is a "clean" steel, with very low levels of impurities, EM10 has higher contents of elements such as Si, Ni, P, which could form clusters, precipitates or segregate at dislocations or grain boundaries because of radiation enhanced and radiation induced phenomena [7–11]. Microstructural investigations and nanoindentation measurements performed on model alloys of low purity have shown the major contribution of impurity clusters to hardening [12].

Investigation of the microstructural evolution under irradiation at the nano-scale is thus of major interest to understand the macroscopic behavior such as hardening or localized corrosion.

This paper reports atom probe tomography (APT) characterizations of EM10 and EUROFER97 alloys irradiated with ions and electrons at 300 °C to doses of 0.15 and 0.6 dpa. Ions and electrons irradiations are alternative irradiation sources to neutron irradiations, which are long, expensive, and access to facilities is restricted. Moreover, using charged particles allows to realize parametric irradiations quite easily.

In a first part, Materials and Methods are presented. In the second part, results of APT experiments performed on irradiated EM10 and EUROFER97 steels are presented and discussed.

Table 1
Nominal chemical composition of the as-received alloys (Optical Emission Spectrometry).

(%at)	Cr	C	Ni	Si	P	N	S	Mo	Mn	Cu	Co	As	W	V	Nb
EM10	9.25	0.447	0.226	0.669	0.034	0.122	0.009	0.553	0.433	0.044	0.019	0.015	0.018	0.239	0.042
E97	9.74	0.422	**0.019**	**0.119**	–	0.163	0.003	**0.006**	0.537	–	–	0.015	**0.372**	0.208	–

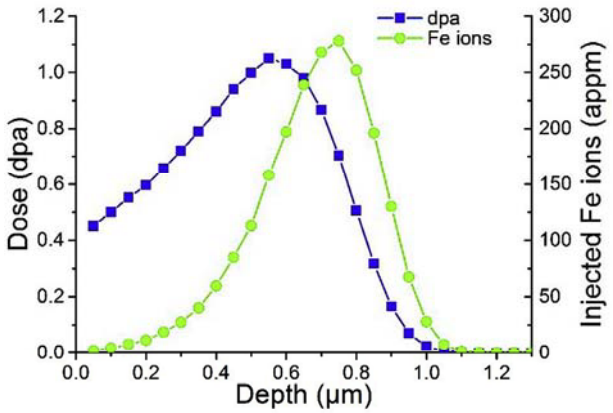

Fig. 1. Evolution with depth of damage and injected interstitials concentration after irradiation with 2 MeV Fe^{2+} ions (calculated with SRIM) [15,16].

Table 2
Clusters' characteristics after different irradiation conditions for EM10 alloys.

	Guinier radius (nm)	Equivalent radius (nm)	Number density (m^{-3})	F_v (%)
Ions 0.6 dpa	1.13 ± 0.29	1.08 ± 0.3	$4.2 \pm 0.7 \times 10^{23}$	0.34 ± 0.1
Electrons 0.15 dpa	1.7 ± 0.25	1.95 ± 0.32	$3.3 \pm 0.6 \times 10^{23}$	1 ± 0.1
Electrons 0.6 dpa	1.45 ± 0.31	1.64 ± 0.33	$3.5 \pm 0.6 \times 10^{23}$	0.93 ± 0.1

2. Materials and Methods

2.1. Materials

The compositions of EM10 and EUROFER 97 (E97) investigated in this work are given in Table 1. E97 (heat number E83698) was forged and rolled to obtain 21 mm plate. Austenitization treatment was performed at 980 °C during 30 min followed by air-cooling.

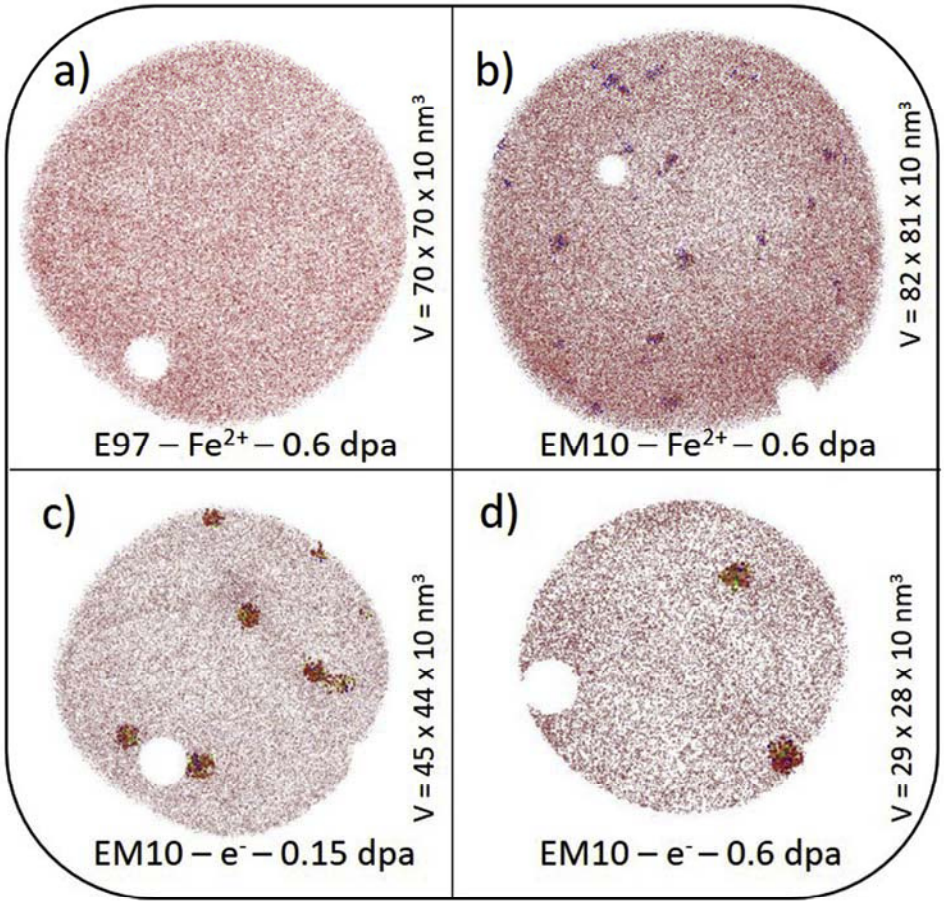

Fig. 2. APT volumes showing Cr atoms in red, Si atoms in blue, Ni atoms in orange, P atoms in green and Mn atoms in Yellow/Green. a) Eurofer97 and b) EM10 alloys both irradiated with Fe2+ ions at 0.6 dpa. EM10 alloys irradiated with electrons at 300 °C to a dose of c) 0.15 dpa and d) 0.6 dpa. Note that precipitates' atoms are shown 20% bigger than matrix atoms. Crystallographic poles have been removed (hole in the volumes) in the analyses to avoid isoconcentration artefacts. (For interpretation of the references to colour in this figure legend, the reader is referred to the Web version of this article.)

Table 3
Clusters main elements composition in EM10 alloy irradiated with Fe ions and Electrons up to dose of 0.6dpa.

	Ions 0.6 dpa	Electrons 0.15 dpa	Electrons 0.6 dpa
Si (at.%)	4.89 ± 0.23	8.91 ± 0.52	13.27 ± 0.30
Ni (at.%)	0.99 ± 0.11	3.39 ± 0.33	14.11 ± 0.31
P (at.%)	0.22 ± 0.05	0.69 ± 0.15	1.47 ± 0.11
Mn (at.%)	0.8 ± 0.1	1.03 ± 0.19	2.98 ± 0.15
Cu (at.%)	0.05 ± 0.02	0.11 ± 0.06	0.18 ± 0.04
Cr (at.%)	9.06 ± 0.31	11.22 ± 0.58	8.24 ± 0.24
Co (at.%)	0.02 ± 0.02	0.085 ± 0.05	0.44 ± 0.06
As (at.%)	0.02 ± 0.02	0.068 ± 0.05	0.19 ± 0.04
Mo (at.%)	0.55 ± 0.08	0.69 ± 0.15	0.63 ± 0.07

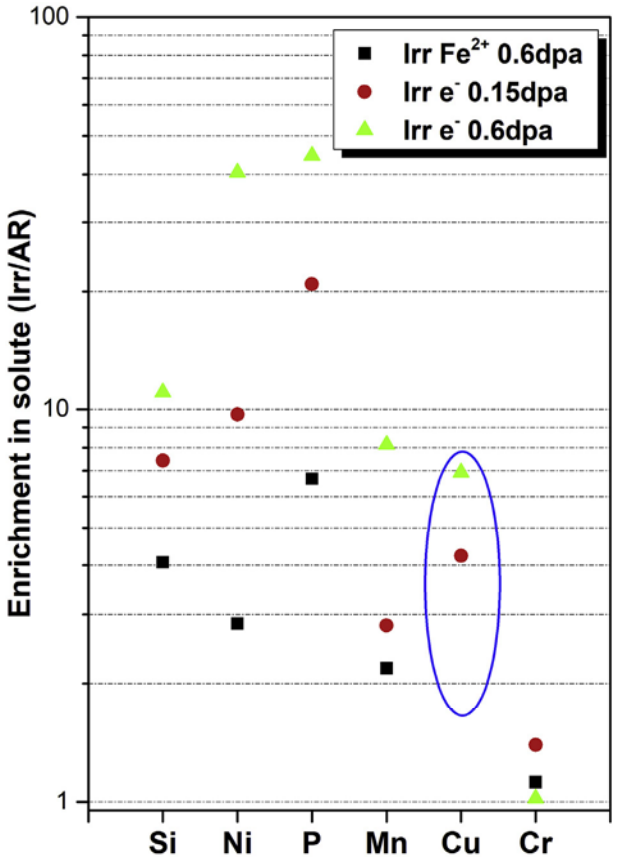

Fig. 3. Enrichment of solute or impurities in clusters in EM10 alloys after ion and electron irradiations at 0.15 (only electrons) and 0.6 dpa Enrichment is calculated according to: $\frac{C_i^{irr}}{C_i^{AR}}$ where AR stands for as-received (before irradiation) and after irradiation.

Then, tempering has been applied at 760 °C for 90 min. EM10 (heat number WH420) was forged and rolled to obtain a plate of 15.5 mm. Then, normalization treatment at 990 °C during 50 min followed by annealing at 750 °C during 1 h was conducted.

3. Irradiations

3.1. . Ion irradiation

Massive discs 100 μm thick and 3 mm in diameter were first mechanically polished and then electro-chemically polished in a solution of 10% perchloric acid, 20% Butoxy − 2 ethanol and 70% ethanol absolute (T = 5 °C, V ≈ 30 V) in order to remove the plastic deformation introduced during mechanical polishing. They were

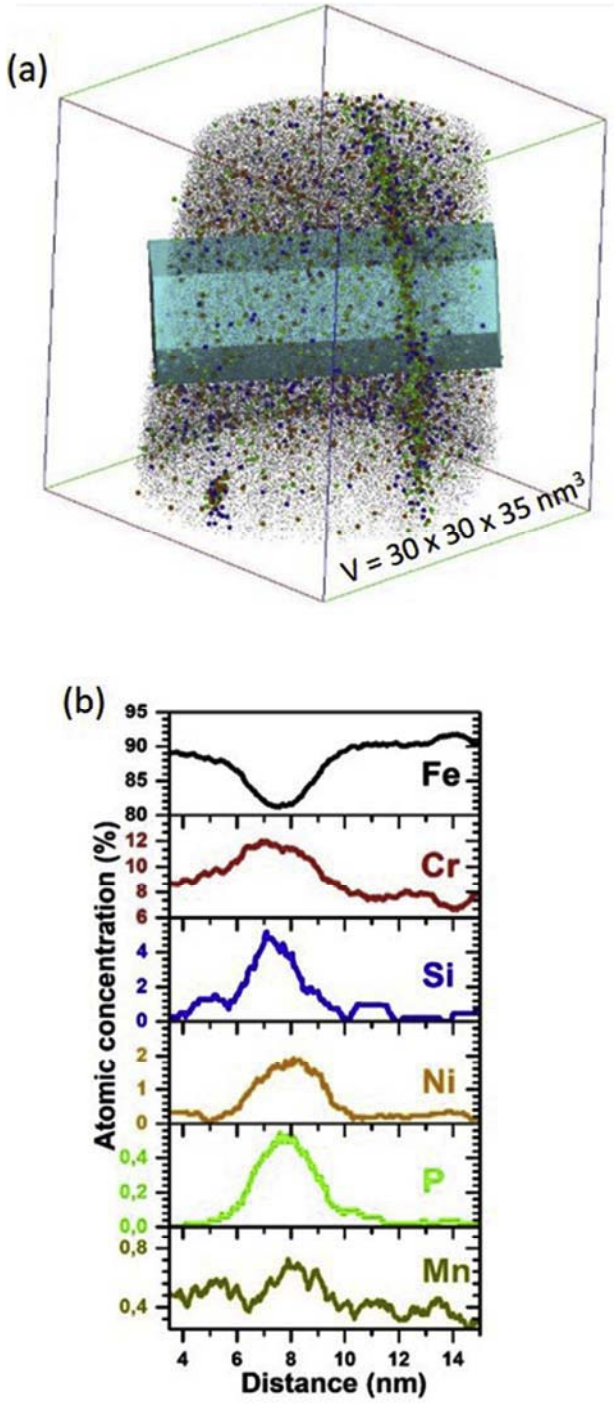

Fig. 4. (a) 3D Atom probe volume with Si atoms (blue), Ni atoms (orange), P atoms (green) and Fe matrix (black spots), (b) concentration profiles of main elements across the grain boundary in an EM10 alloy irradiated with electron at a dose of 0.15 dpa at 300 °C. (For interpretation of the references to colour in this figure legend, the reader is referred to the Web version of this article.)

irradiated with 2 MeV Fe^{2+} ions at 300 °C using the JANNuS-Saclay facility [13,14]. The irradiation temperature was measured with three thermocouples and an infrared camera. The ions flux, measured with six faraday cups, was 5.4×10^{10} ions/($cm^2 \cdot s$) and the fluence was 9.2×10^{14} ions/(cm^2). The damage and implantation profiles, given in Fig. 1, were calculated with SRIM (Stopping and Range of Ions in Matter) [15,16] using the "Quick" Kinchin and

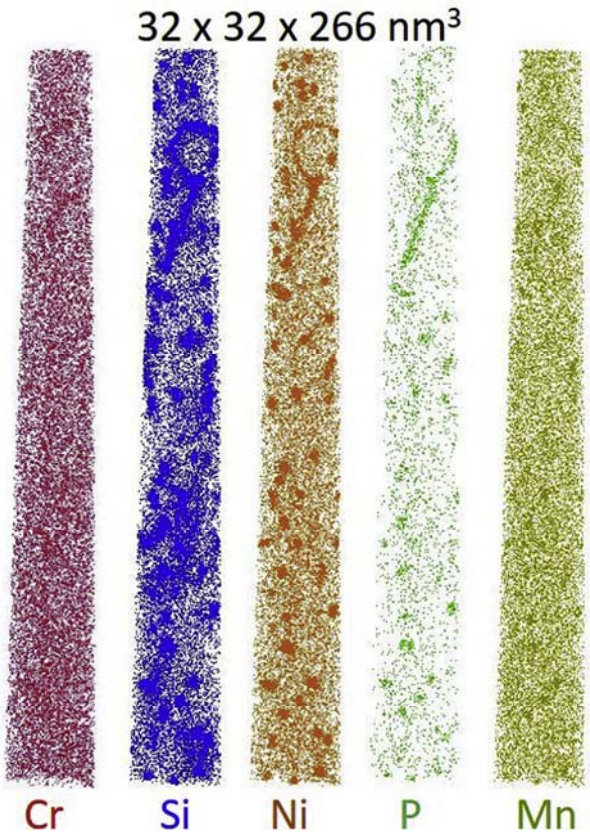

Fig. 5. APT volumes of the EM10 alloy irradiated with electrons to a dose of 0.6 dpa at 300 °C.

Pease option as recommended by Stoller et al. [17] and a displacement threshold of 40 eV [18]. The dose rate varied from 3×10^{-5}dpa/s near the surface up to 6.1×10^{-5} dpa/s at the damage peak. The APT samples were lifted out using a Helios 650 NanoLab FEI Focused Ion Beam (FIB) at 150 nm depth (0.55 dpa). The final milling was performed with a Ga beam energy of 2 kV in order to reduce implantation of Ga ions in the material.

3.2. . Electron irradiations

Electron Irradiations were performed using a 1 MeV High Voltage Electron Microscope. The electron flux was 3.55×10^{18} electrons/(cm^2.s) and the calculated doses, using a displacement threshold energy of 40 eV [19,20], were 0.15 and 0.6 dpa (damage rate 3.9 10^{-5} dpa/s). All samples were irradiated at 300 °C, measured with a thermocouple placed in contact with the sample. The APT samples were irradiated using a sample holder that was specifically designed for HVEM irradiation of needle-shaped APT samples. To limit surface effects (such as point defects migration and elimination at free surfaces) occurring when the area of interest is too close to the tip surface, needles with large tip radius (1–2 μm) were irradiated. They were obtained by choosing suitable electro polishing conditions (75% acetic acid −25% perchloric acid, 7 to 5V and 98% ether – 2% perchloric acid 7V). After irradiation, the samples were annular milled using a Helios 650 NanoLab FEI Focused Ion Beam (FIB) in order to obtain needles suitable for APT analysis (tip radius ≈50 nm). However, as the thickness of the irradiated samples was significantly larger than the thickness of TEM thin foils (typically a few 100 nm), usually used for electron irradiations in the HVEM, the expected beam heating is higher. Based on finite element calculations, beam heating was evaluated to be limited to 29 °C for our experimental conditions. The tips were placed perpendicular to the electron beam and a 6–8 μm zone of the samples was irradiated.

4. Experimental methods

The samples were analyzed using a LEAP 4000X HR Atom Probe from CAMECA having a high mass resolution and a detector efficiency of 42%. The samples were analyzed at a temperature of 80K to prevent excessive rupture of the specimen under analysis. During analyses, the atom probe specimens were electrically pulsed with a pulse fraction of 20%, a pulse rate of 200 kHz and a detection rate of 0.002 atom per pulse. Reconstructions of the volumes were done with IVAS 3.6.12 (CAMECA software) using the following parameters: a compression factor of 1.4–1.5, an evaporation field of 33 V nm^{-1} and a k factor between 3.25 and 4.5. k parameter was deduced from the calibration of the [110] interplanar distance in the crystallographic pole.

Data treatments were performed thanks to the 3D Data Software for Atom Probe Tomography developed by the GPM research group in Rouen, France. Measurement of the size and number density of clusters was performed using the “iso-position” concentration data filter [21–23]. The filter enables to distinguish the particles from the surrounding matrix owing to their chemical composition. The parameters used were: concentration threshold X_{Si}>3 at.% for ions irradiation and X_{Si}>7.2 at.% for electrons irradiated samples, grid pattern of 1.0 nm, separation distance d = 0.2 nm and a minimum number of atoms in the particles of 100. The cluster composition was measured in the core of each cluster to eliminate the compositional dependence on the threshold value. Composition values were averaged over all the measurements. The number density of the particles was determined by a simple ratio of the number of observed clusters to the overall analyzed volume. The radius of each cluster was deduced from the number of atoms in each particle considering spherical particles (equivalent radius): $R = \sqrt[3]{\frac{3nV_{at}}{4\pi Q}}$ with V_{at} the Fe atomic volume and Q the detector efficiency. The Guinier radius have also been measured. The volume fraction was defined as the ratio of the number of atoms inside the clusters to the total number of collected atoms. The basic principle of APT and data treatment may be found in different books or reviews [23–27].

5. Results and discussion

5.1. Ions irradiations (0.6 dpa)

APT volumes of EM10 and E97 after ion irradiation at a dose of 0.6 dpa are shown in Fig. 2. EM10 alloy exhibits clusters whereas the 3D atom maps of E97 are homogenous. The EM10 clusters characteristics are reported in Table 2. Their composition is provided in Table 3. Note that Mo concentration is similar to Mo concentration in the matrix. Its effect on clustering was thus thought to be insignificant. Enrichment ($\frac{C_i^{Irr}}{C_i^{AR}}$ where AR stands for as-received) of the main elements is reported in Fig. 3. The highest enrichment is observed for P. Similarly to prior work [28] on Fe– 9% Cr model alloys of low purity, Cr enrichment appears very small if any. On contrary, P, Ni, and Si enrichments are much lower in our case than the values reported in Ref. [28] (184 for P, 7 for Ni and 32.3 for Si). According to the bell-shaped temperature dependence reported by Pareige et al. [28] higher enrichments would have been expected as the dose rate in the present work (≈10^{-5} dpa.s^{-1}) is lower than in Ref. [28] (≈10^{-4} dpa.s^{-1}). This behavior is not fully understood yet.

As shown in Fig. 2, no clusters were observed in E97 whereas

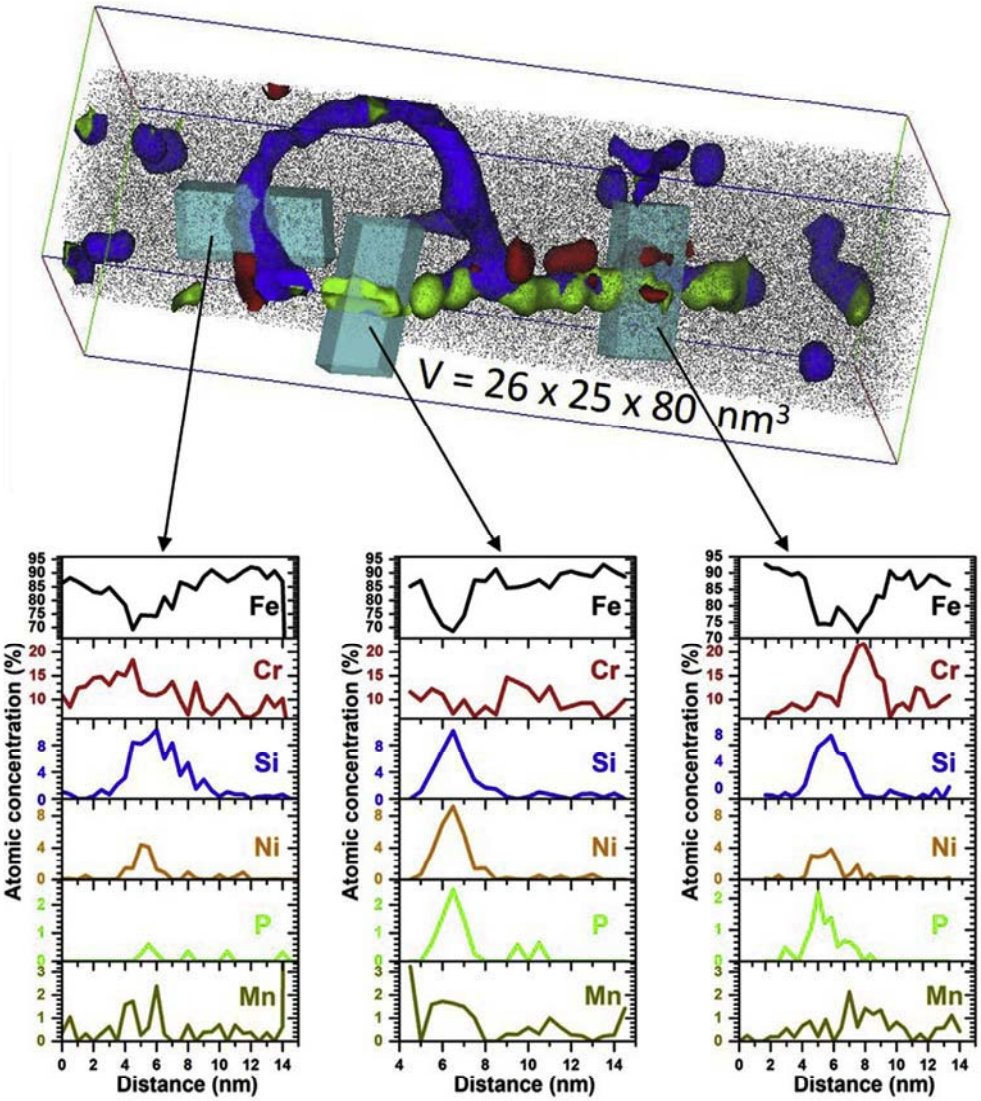

Fig. 6. (a) Dislocation/dislocation loop in an EM10 alloy irradiated with electron to a dose of 0.6 dpa at 300 °C. Iso concentration of Si (blue) at 4.5 at.%, Cr (red) at 16 at.% and P (green) at 0.7 at.% were done. (b, c and d) linear concentration profiles throught a box of $3 \times 7 \times 15$ nm^3 (slice of 0.5 nm). (For interpretation of the references to colour in this figure legend, the reader is referred to the Web version of this article.)

clusters formed in EM10. P could be at the origin of this different behavior. Indeed, P is absent in EUROFER97 whereas P atoms strongly enrich clusters observed in EM10. This agrees with the conclusions of Pareige et al. [28], Meslin et al. [29] and Domain et al. [30] which considered P as a stabilizer for clusters of point defects. This means that the observed clusters were likely to form heterogeneously on point defects clusters. Our work strongly suggest that without P cluster formation does not take place. Although the initial amount of P is low in EM10 (0.034 at.%), its effect on microstructural evolution seems of major importance. Nevertheless, clusters enriched in Cr and Mn were observed in E97 irradiated with neutrons [31].

6. Electrons irradiations

Electron irradiations were carried out only on EM10.The microstructure has been characterized at two doses: 0.15 dpa and 0.6 dpa. The second dose allows direct comparison with ion irradiation. As shown by Fig. 2, clusters are formed at both doses. Radius, number densities and volume fractions of clusters are quite similar at the two doses (Table 2). Composition is given in Table 3. The dose does not seem to have an impact on the clusters' spatial characteristics but on their chemical composition. Fig. 3 and Table 3 reveal that at the same dose, clustering is much more efficient under electron irradiation: size, volume fraction and concentration are higher under electron irradiation. This is due to the much higher fraction of isolated points defects created under electron irradiation for a given dpa value [32]. As already shown in FeCr alloys, electron irradiation is more efficient to enhance diffusion as all defects are created as isolated point defects [33]. Moreover, point defects clusters are created in the displacement cascades under ion irradiation leading to larger increase in sink density for point defects, which in turn decrease the fraction of isolated point defects.

After electron irradiation, clusters are also enriched in Cu whereas no Cu has been detected in clusters after ion irradiation. This element presents a strong tendency to solute-drag by vacancies leading to Cu segregation at sinks such as point defects

clusters [34–38]. Because of higher concentration of free point defects under electron irradiation, flux coupling is more efficient. This is in good agreement with the behavior of Ni, Si, Mn and P which also present strong dragging tendencies [38–41] and for which enrichment under electron irradiation is higher than under ion irradiation. Co and As enrichment have also been measured. An enrichment of Co of 4.7 at a dose of 0.15 dpa and 25.6 at a dose of 0.6 dpa was measured. For As, enrichment of 5.5 (0.15 dpa) and 15.6 (0.6 dpa) is observed. To our knowledge, it is the first time that enrichments in these elements are found in clusters formed under irradiation in F/M steels.

In general, enrichment values were bigger at 0.6 than 0.15 dpa. This is consistent with the diffusion process, which is more efficient at 0.6 dpa. Cr enrichment is an exception, as it seems to decrease with dose. Different hypothesis could be made but the more likely is that there are some uncertainties on measurements.

7. Radiation induced segregation after electrons irradiation

Fig. 4(a) shows a 3D APT volume of EM10 alloy irradiated with electrons at a dose of 0.15 dpa at 300 °C. As can be seen, segregation of Si, Ni, P, Cr and Mn atoms is observed at a grain boundary (GB). The main chemical elements present at the GB are the same as the ones observed in clusters. No clusters have been observed in the vicinity of the GB. According to Fig. 4 (a) the cluster free zone is of at least 20 nm. This free zone is due to the interaction between point defect depletion and segregation. The segregation could be induced by radiation or be a thermal/equilibrium pre-existing segregation. In FeCr alloys, it has been simulated by Soisson et al. [42] and observed experimentally by Kuksenko et al. [11].

Fig. 5 shows the microstructure of the EM10 alloy irradiated with electrons containing SiNiPMn enriched clusters and a dislocation/dislocation loop.

Fig. 6 presents a zoom on the dislocation lines pined on a dislocation loop observed in Fig. 5. Fig. 6(b, c and d) presents different concentration profiles drawn across the dislocation line and dislocation loop. As for clusters, Si, Ni, P, Mn and Cr are observed to enrich at these defects. Cr clusters are observed to be linked to the dislocation loop and to the line. On the concentration profiles c) and d) it can be observed that Cr maximum is shifted with respect to Si, Ni, P maximum. Such behavior has already been reported by Kuksenko et al. [11,43]. Cr atoms being oversized atoms, they segregate in tension zone [11,44,45]. Si, Ni and P would be therefore situated in the compression zone. Mn atoms seems to be located both in the tension and compression zones. A small amount of Mn (between 0.3 and 1.5 at.%) is observed to enrich the Cr clusters.

P atoms do not segregate uniformly all along the loop (Figs. 5 and 6). P segregation is higher along the dislocation lines. Note that in both the GB and the dislocation, the number of atoms is about 1.4 times higher than in the matrix. This is the result of the well-known APT artefact of ions trajectory focusing due to different evaporation field behaviors of regions with different composition and/or crystallography.

8. Conclusion

In summary, an EM10 and a Eurofer alloys were irradiated with ions Fe^{2+} and electrons at doses up to 0.6 dpa. APT characterizations shown that:

- No precipitation was detected in E97 alloy after ions irradiation;
- EM10 alloy exhibits SiNiPMn clusters under ion irradiation and SiNiPMn–Cu clusters under electron irradiations;
- P seems to be necessary to the formation of the solute clusters;
- Si, Ni, P, Mn, Cr segregate at GB and dislocation line and loop.

Declaration of competing interest

The authors declare that they have no known competing financial interests or personal relationships that could have appeared to influence the work reported in this paper.

CRediT authorship contribution statement

O. Tissot: Writing - original draft, Formal analysis, Visualization. **G. Sakr:** Investigation, Formal analysis. **C. Pareige:** Writing - review & editing. **J. Henry:** Writing - review & editing, Supervision.

Acknowledgements

The experiment were done using both JANNuS-Saclay (Joint Accelerators for Nanoscience and Nuclear Simulation), and the EM7 HVEM at CEA Saclay, France and supported by the French Network EMIR. This work received assistance from the “Agence Nationale de la Recherche” program GENESIS referenced as ANR-11-EQPX-0020. The authors also acknowledge I. Mouton for fruitful discussion on APT data treatment.

Appendix A. Supplementary data

Supplementary data to this article can be found online at https://doi.org/10.1016/j.jnucmat.2020.151995.

References

[1] C. Fazio, P. Dubuisson, Proc. Int. Conf. Fast React. Relat. Fuel Cycles Safe Technol. Sustain. Scenar. 1 (2013) 487.
[2] P. Dubuisson, D. Gilbon, J.L. Séran, Microstructural evolution of ferritic-martensitic steels irradiated in the fast breeder reactor Phénix, J. Nucl. Mater. 205 (1993) 178–189, https://doi.org/10.1016/0022-3115(93)90080-I.
[3] F.A. Garner, M.B. Toloczko, B.H. Sencer, Comparison of swelling and irradiation creep behavior of fcc-austenitic and bcc-ferritic/martensitic alloys at high neutron exposure, J. Nucl. Mater. 276 (2000) 123–142, https://doi.org/10.1016/S0022-3115(99)00225-1.
[4] R. Lindau, A. Möslang, M. Rieth, M. Klimiankou, E. Materna-Morris, A. Alamo, A.-A.F. Tavassoli, C. Cayron, A.-M. Lancha, P. Fernandez, N. Baluc, R. Schäublin, E. Diegele, G. Filacchioni, J.W. Rensman, B.v. d. Schaaf, E. Lucon, W. Dietz, Present development status of EUROFER and ODS-EUROFER for application in blanket concepts, Fusion Eng. Des. 75–79 (2005) 989–996, https://doi.org/10.1016/j.fusengdes.2005.06.186.
[5] O.J. Weiß, E. Gaganidze, J. Aktaa, Quantitative characterization of microstructural defects in up to 32dpa neutron irradiated EUROFER97, J. Nucl. Mater. 426 (2012) 52–58, https://doi.org/10.1016/j.jnucmat.2012.03.027.
[6] J. Henry, X. Averty, A. Alamo, Tensile and impact properties of 9Cr tempered martensitic steels and ODS-FeCr alloys irradiated in a fast reactor at 325 °C up to 78 dpa, J. Nucl. Mater. 417 (2011) 99–103, https://doi.org/10.1016/j.jnucmat.2010.12.203.
[7] Z. Jiao, V. Shankar, G.S. Was, Phase stability in proton and heavy ion irradiated ferritic–martensitic alloys, J. Nucl. Mater. 419 (2011) 52–62, https://doi.org/10.1016/j.jnucmat.2011.08.020.
[8] J.P. Wharry, Z. Jiao, V. Shankar, J.T. Busby, G.S. Was, Radiation-induced segregation and phase stability in ferritic–martensitic alloy T 91, J. Nucl. Mater. 417 (2011) 140–144, https://doi.org/10.1016/j.jnucmat.2010.12.052.
[9] J.P. Wharry, Z. Jiao, G.S. Was, Application of the inverse Kirkendall model of radiation-induced segregation to ferritic–martensitic alloys, J. Nucl. Mater. 425 (2012) 117–124, https://doi.org/10.1016/j.jnucmat.2011.10.035.
[10] V. Kuksenko, C. Pareige, P. Pareige, Cr precipitation in neutron irradiated industrial purity Fe–Cr model alloys, J. Nucl. Mater. 432 (2013) 160–165, https://doi.org/10.1016/j.jnucmat.2012.07.021.
[11] V. Kuksenko, C. Pareige, C. Genevois, P. Pareige, Characterisation of Cr, Si and P distribution at dislocations and grain-boundaries in neutron irradiated Fe–Cr model alloys of low purity, J. Nucl. Mater. 434 (2013) 49–55, https://doi.org/10.1016/j.jnucmat.2012.11.027.
[12] F. Bergner, C. Pareige, V. Kuksenko, L. Malerba, P. Pareige, A. Ulbricht, A. Wagner, Critical assessment of Cr-rich precipitates in neutron-irradiated Fe–12at%Cr: comparison of SANS and APT, J. Nucl. Mater. 442 (2013) 463–469, https://doi.org/10.1016/j.jnucmat.2013.05.023.
[13] Y. Serruys, P. Trocellier, S. Miro, E. Bordas, M.O. Ruault, O. Kaïtasov, S. Henry,

O. Leseigneur, T. Bonnaillie, S. Pellegrino, S. Vaubaillon, D. Uriot, JANNUS: a multi-irradiation platform for experimental validation at the scale of the atomistic modelling, J. Nucl. Mater. 386–388 (2009) 967–970, https://doi.org/10.1016/j.jnucmat.2008.12.262.
[14] L. Beck, Y. Serruys, S. Miro, P. Trocellier, E. Bordas, F. Leprêtre, D. Brimbal, T. Loussouarn, H. Martin, S. Vaubaillon, S. Pellegrino, D. Bachiller-Perea, Ion irradiation and radiation effect characterization at the JANNUS-Saclay triple beam facility, J. Mater. Res. 30 (2015) 1183–1194, https://doi.org/10.1557/jmr.2014.414.
[15] J.F. Ziegler, M.D. Ziegler, J.P. Biersack, SRIM — the stopping and range of ions in matter, Nucl. Instrum. Methods Phys. Res. Sect. B Beam Interact. Mater. Atoms 268 (2010) (2010) 1818–1823, https://doi.org/10.1016/j.nimb.2010.02.091.
[16] J.F. Ziegler, J.P. Biersack, U. Littmark, The Stopping and Range of Ions in Matter, Pergamon Press, 1985.
[17] R.E. Stoller, M.B. Toloczko, G.S. Was, A.G. Certain, S. Dwaraknath, F.A. Garner, On the use of SRIM for computing radiation damage exposure, Nucl. Instrum. Methods Phys. Res. Sect. B Beam Interact. Mater. Atoms 310 (2013) 75–80, https://doi.org/10.1016/j.nimb.2013.05.008.
[18] ASTM E693, 12 Standard Practice for Characterizing Neutron Exposures in Iron and Low Alloy Steels in Terms of Displacements Per Atom (DPA), Annu. Book ASTM Stand. (1994) E 706, 12.02.
[19] K. Nordlund, J. Wallenius, L. Malerba, Molecular dynamics simulations of threshold displacement energies in Fe, Nucl. Instrum. Methods Phys. Res. Sect. B Beam Interact. Mater. Atoms 246 (2006) 322–332, https://doi.org/10.1016/j.nimb.2006.01.003.
[20] R.E. Stoller, M.B. Toloczko, G.S. Was, A.G. Certain, S. Dwaraknath, F.A. Garner, On the use of SRIM for computing radiation damage exposure, Nucl. Instrum. Methods Phys. Res. Sect. B Beam Interact. Mater. Atoms 310 (2013) 75–80, https://doi.org/10.1016/j.nimb.2013.05.008.
[21] C. Pareige, V. Kuksenko, P. Pareige, Behaviour of P, Si, Ni impurities and Cr in self ion irradiated Fe–Cr alloys – comparison to neutron irradiation, J. Nucl. Mater. 456 (2015) 471–476, https://doi.org/10.1016/j.jnucmat.2014.10.024.
[22] E. Meslin, B. Radiguet, M. Loyer-Prost, Radiation-induced precipitation in a ferritic model alloy: an experimental and theoretical study, Acta Mater. 61 (2013) 6246–6254, https://doi.org/10.1016/j.actamat.2013.07.008.
[23] W. Lefebvre-Ulrikson, F. Vurpillot, X. Sauvage (Eds.), Atom Probe Tomography, Academic Press, 2016. https://www.sciencedirect.com/science/article/pii/B9780128046470010019. accessed February 2, 2017.
[24] D.J. Larson, T.J. Prosa, R.M. Ulfig, B.P. Geiser, T.F. Kelly, Local Electrode Atom Probe Tomography, Springer New York, New York, NY, 2013. http://link.springer.com/10.1007/978-1-4614-8721-0. accessed April 26, 2016.
[25] M.P. Moody, J.M. Cairney, B. Gault, S.P. Ringer, Atom Probe Microscopy, vol. 160, Springer Series in Materials Science, 2012. http://www.springer.com/materials/characterization+%26+evaluation/book/978-1-4614-3435-1. accessed October 24, 2012.
[26] M. Miller, A. Cerezo, M. Hetherington, G. Smith, Atom Probe Field Ion Microscopy, Clarendon, Oxford, 1996.
[27] M. Miller, Atom Probe Tomography, Kluwer Academic/Plenium Publishers, New York., 2000.
[28] C. Pareige, V. Kuksenko, P. Pareige, Behaviour of P, Si, Ni impurities and Cr in self ion irradiated Fe–Cr alloys – comparison to neutron irradiation, J. Nucl. Mater. 456 (2015) 471–476, https://doi.org/10.1016/j.jnucmat.2014.10.024.
[29] E. Meslin, C.-C. Fu, A. Barbu, F. Gao, F. Willaime, Theoretical study of atomic transport via interstitials in dilute $\mathrm{Fe}\text{-}\mathrm{P}$ alloys, Phys. Rev. B. 75 (2007), 94303, https://doi.org/10.1103/PhysRevB.75.094303.
[30] C. Domain, C.S. Becquart, Diffusion of phosphorus in $\ensuremath{\alpha}\text{\ensuremath{-}}\mathrm{Fe}$: an ab initio study, Phys. Rev. B. 71 (2005), 214109, https://doi.org/10.1103/PhysRevB.71.214109.
[31] S.V. Rogozhkin, A.A. Nikitin, A.A. Aleev, A.B. Germanov, A.G. Zaluzhnyi, Atom probe study of radiation induced precipitates in Eurofer97 Ferritic-Martensitic steel irradiated in BOR-60 reactor, Inorg. Mater. Appl. Res. 4 (2013) 112–118.
[32] G.S. Was, T. Allen, Radiation-induced segregation in multicomponent alloys : effect of particle type, Mater. Char. 32 (1994) 239–255.
[33] O. Tissot, C. Pareige, E. Meslin, B. Decamps, J. Henry, Kinetics of α' precipitation in an electron-irradiated Fe15Cr alloy, Scr. Mater. 122 (2016) 31–35, https://doi.org/10.1016/j.scriptamat.2016.05.021.
[34] E. Vincent, C.S. Becquart, C. Domain, Ab initio calculations of vacancy interactions with solute atoms in bcc Fe, Nucl. Instrum. Methods Phys. Res. Sect. B Beam Interact. Mater. Atoms 228 (n.d.) 137–141.
[35] B. Radiguet, A. Barbu, P. Pareige, Understanding of copper precipitation under electron or ion irradiations in FeCu0.1wt% ferritic alloy by combination of experiments and modelling, J. Nucl. Mater. 360 (2007) 104–117, https://doi.org/10.1016/j.jnucmat.2006.09.007.
[36] P. Pareige, B. Radiguet, A. Barbu, Heterogeneous irradiation-induced copper precipitation in ferritic iron–copper model alloys, J. Nucl. Mater. 352 (2006) 75–79, https://doi.org/10.1016/j.jnucmat.2006.02.073.
[37] F. Soisson, C.C. Fu, Atomistic simulations of copper precipitation and radiation induced segregation in α-iron, Solid State Phenom. 139 (2008) 107–112.
[38] L. Messina, M. Nastar, T. Garnier, C. Domain, P. Olsson, Exact ab initio transport coefficients in bcc $\mathrm{Fe}\ensuremath{-}X$ ($X=\mathrm{Cr}$, Cu, Mn, Ni, P, Si) dilute alloys, Phys. Rev. B. 90 (2014), 104203, https://doi.org/10.1103/PhysRevB.90.104203.
[39] Y. Nagai, K. Takadate, Z. Tang, H. Ohkubo, H. Sunaga, H. Takizawa, M. Hasegawa, Positron annihilation study of vacancy-solute complex evolution in Fe-based alloys, Phys. Rev. B. 67 (2003), 224202, https://doi.org/10.1103/PhysRevB.67.224202.
[40] A.V. Barashev, Monte Carlo simulation of phosphorus diffusion in α-iron via the vacancy mechanism, Philos. Mag. 85 (2005) 1539–1555, https://doi.org/10.1080/14786430500036348.
[41] L. Messina, M. Nastar, N. Sandberg, P. Olsson, Systematic electronic-structure investigation of substitutional impurity diffusion and flux coupling in bcc iron, Phys. Rev. B. 93 (2016), https://doi.org/10.1103/PhysRevB.93.184302.
[42] F. Soisson, T. Jourdan, Radiation-accelerated precipitation in Fe–Cr alloys, Acta Mater. 103 (2016) 870–881, https://doi.org/10.1016/j.actamat.2015.11.001.
[43] V. Kuksenko, C. Pareige, P. Pareige, Intra granular precipitation and grain boundary segregation under neutron irradiation in a low purity Fe–Cr based alloy, J. Nucl. Mater. 425 (2012) 125–129, https://doi.org/10.1016/j.jnucmat.2011.10.031.
[44] E.E. Zhurkin, D. Terentyev, M. Hou, L. Malerba, G. Bonny, Metropolis Monte-Carlo simulation of segregation in Fe–Cr alloys, J. Nucl. Mater. 417 (2011) 1082–1085, https://doi.org/10.1016/j.jnucmat.2010.12.191.
[45] L. Malerba, G. Bonny, D. Terentyev, E.E. Zhurkin, M. Hou, K. Vörtler, K. Nordlund, Microchemical effects in irradiated Fe–Cr alloys as revealed by atomistic simulation, J. Nucl. Mater. 442 (2013) 486–498, https://doi.org/10.1016/j.jnucmat.2012.12.038.